Strengthening of Poly(butylene adipate-*co*-terephthalate) by Melt Blending with a Liquid Crystalline Polymer

Yuko Iwakura, Yongjin Li, Kazuo Nakayama, Hiroshi Shimizu

Nanotechnology Research Institute, National Institute of Advanced Industrial Science and Technology (AIST), Tsukuba Central 5, 1-1-1 Higashi, Tsukuba, Ibaraki 305-8565, Japan

Received 30 September 2007; accepted 20 December 2007
DOI 10.1002/app.28123
Published online 28 March 2008 in Wiley InterScience (www.interscience.wiley.com).

ABSTRACT: Poly(butylene adipate-*co*-terephthalate) (PBAT) is a soft biodegradable polymer with a low melting temperature. PBAT has been melt-blended with a liquid crystalline polymer (LCP) aiming at preparing a new biodegradable polymer blend with improved mechanical properties. The phase structure and crystalline morphologies of the PBAT/LCP blends were investigated using scanning electron microscopy (SEM), differential scanning calorimetry (DSC), small-angle X-ray scattering (SAXS), and transmission electron microscopy (TEM). It was found that the LCP domains are precisely dispersed in the PBAT matrix and that these domains act as the nuclei for PBAT crystallization. The nonisothermal crystallization temperature from the melt was dramatically shifted from 50°C to about 95°C by the addition of 20% LCP. In addition, the tensile modulus of the prepared blends increases gradually with increasing LCP content, indicating the excellent strengthening effects of LCP on the PBAT matrix. © 2008 Wiley Periodicals, Inc. J Appl Polym Sci 109: 333–339, 2008

Key words: poly (butylene adipate-*co*-terephthalate) (PBAT); liquid crystalline polyme (LCP); morphology; mechanical properties

INTRODUCTION

With an increase in concern for the global environment, many investigations on biodegradable aliphatic polyesters, such as poly(lactic acid) (PLA), poly(glycolic acid) (PGA), poly(epsilon caprolactone) (PCL), poly(3-hydroxybutyrate) (PHB), and poly(butylene succinate) (PBS), are in progress.[1–6] Poly(butylene adipate-*co*-terephthalate) (PBAT) is an aliphatic–aromatic copolyester, which is fully biodegradable.[7] Its biodegradation behavior and properties have been reported by Müller and coworkers.[8–11] PBAT is a flexible plastic designed for film extrusion and extrusion coating. However, its low strength and low heat resistance are major drawbacks for many applications. Blending of different polymers has been considered to be an excellent method of developing new materials, often exhibiting combinations of properties superior to either of the pure components. PBAT has been blended with several polymers, for example, PBT, PLA, and starch,[12–14] but it was only used as the minor component to modify the mechanical properties of other polymers. Few works have been carried out to improve the mechanical properties of PBAT itself.

On the other hand, many studies have been carried out on the *in situ* reinforcement of a thermoplastic plastic by liquid crystalline polymers (LCPs).[15–19] LCPs are known to have superior physical properties. Moreover, LCP can also deform into fine and elongated fibrils within an isotropic matrix under suitable processing conditions. The LCP blends exhibit high strength and modulus, improved heat resistance and chemical resistance, and a low coefficient of thermal expansion. In view of its high strength and modulus, LCP is considered to be a good candidate for the strengthening of PBAT. In this work, we first try to use LCP as a reinforcement additive for the biodegradable PBAT. The mechanical properties, morphologies, and crystallization behaviors of the composites have been systematically investigated.

EXPERIMENTAL

Materials

The poly(butylene adipate-*co*-terephthalate) (PBAT) used in this study is a commercialized aliphatic-*co*-aromatic biodegradable copolymer from BASF Japan, designated as Ecoflex. It is an ideal random copolymer with 56 mol % butylenes adipate unit. The liquid crystalline polymer (LCP) used is Rodrun 3000

Correspondence to: Y. Li (yongjin-li@aist.go.jp).
Contract grant sponsors: Japan Industrial Technology Association (JITA), New Energy and Industrial Technology Development Organization (NEDO).

Journal of Applied Polymer Science, Vol. 109, 333–339 (2008)

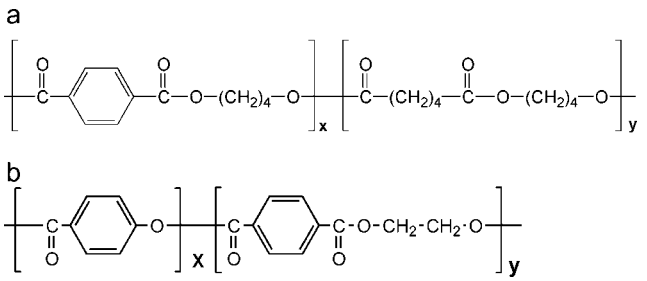

Figure 1 Schematic chemical formulae of (a) PBAT and (b) LCP.

from Unitika. The LCP has a comonomer composition of 60 mol % hydroxybenzoic acid (HBA) and 40 mol % poly(ethylene terephthalate) (PET). The chemical formulae of PBAT and LCP are shown in Figure 1.

Sample preparation

The PBAT pellets were dried under vacuum at 60°C for 12 h and LCP pellets were dried at 90°C for 12 h before blending. The pellets were melt-blended in a variety of the PBAT/LCP compositions by a corotating twin-screw mixer (Toyoseiki Co. KF70V) at 230°C with a screw rotation speed of 200 rpm. The obtained samples were then hot pressed at 210°C to a thin sheet with a thickness of the 500 μm, followed by rapid quenching in ice water. After the melt blending, the PBAT/LCP (=60/40) sample was pelletized and was dried in a vacuum for 24 h at 70°C. Blend sheets were obtained by injection molding at 210°C.

Characterizations

The morphology of the PBAT/LCP blends was investigated by scanning electron microscopy (SEM) (Philip, XL-20 SEM). Specimens were kept in liquid nitrogen for some time and brittle-fractured in liquid nitrogen.

Transmission electron microscopy (TEM) was employed to observe the PBAT crystal morphology in the blends. The specimens were stained using ruthenium tetraoxide (RuO_4) vapor to give for 3 h and then were microtomed at 1 mm/s with the diamond knife at room temperature, to give 70-nm thick sections. Micrographs were taken with a Hitachi H7000 transmission electron microscope operated at 75 kV.

Dynamic mechanical analysis (DMA) was performed on Rheovibron DDV-25FP (Orientec Co. Ltd.

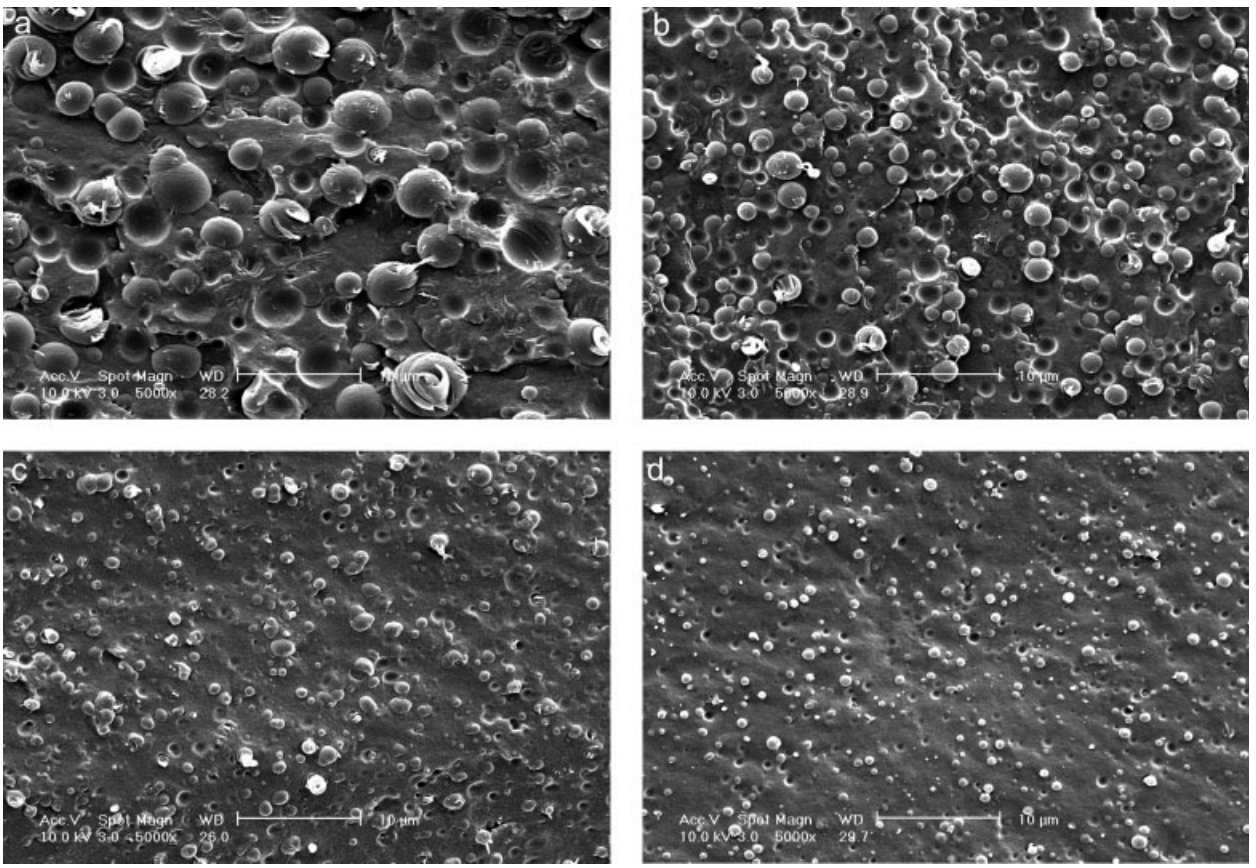

Figure 2 SEM micrographs for the PBAT/LCP blends: (a) PBAT/LCP (=50/50), (b) PBAT/LCP (=60/40), (c) PBAT/LCP (=70/30), and (d) PBAT/LCP (=80/20).

Japan) in a tensile mode. The experiments were carried out at a heating rate of 3°C/min and a frequency of 1 Hz.

Differential scanning calorimetry (DSC) was carried out under nitrogen flow at a heating or cooling rate of 10°C/min with a Perkin–Elmer DSC-7 differential scanning calorimeter calibrated with the melting temperature of indium and zinc. The DSC curves were normalized by sample weight after baseline correction. Crystallization kinetics studies were also carried out with the differential scanning calorimeter. The pure PBAT and PBAT/LCP (=80/20) blend samples were first heated to 200°C, kept at this temperature for 3 min and then cooled (200°C/min) to 78 and 120°C, respectively, for isothermal crystallization.

The tensile mechanical properties were measured following the JIS K7113 standard using a tensile testing machine, Tensilon 10T (Orientec Co. Ltd. Japan), at a crosshead speed of 10 mm/min. A strain recovery test was also performed as follows. After the preset strain (=100% elongation) was attained, the crosshead returned at the same speed as when stretching until zero stress was reached.

Small-angle X-ray scattering (SAXS) patterns were obtained by microfocused Cu Kα radiation (45 kV, 60 mA) generated by an X-ray diffractometer Ultrax 4153A 172B (Rigaku Co. Ltd. Japan). The SAXS images were detected with an imaging plate detector RAXIS-DS3C (Rigaku Co. Ltd. Japan) and then transformed into SAXS profiles by Lorentz-correction analysis.

RESULTS AND DISCUSSION

Phase structures

The phase structure of the blends with different compositions was investigated using SEM, as shown in Figure 2. The bright domains indicate the LCP

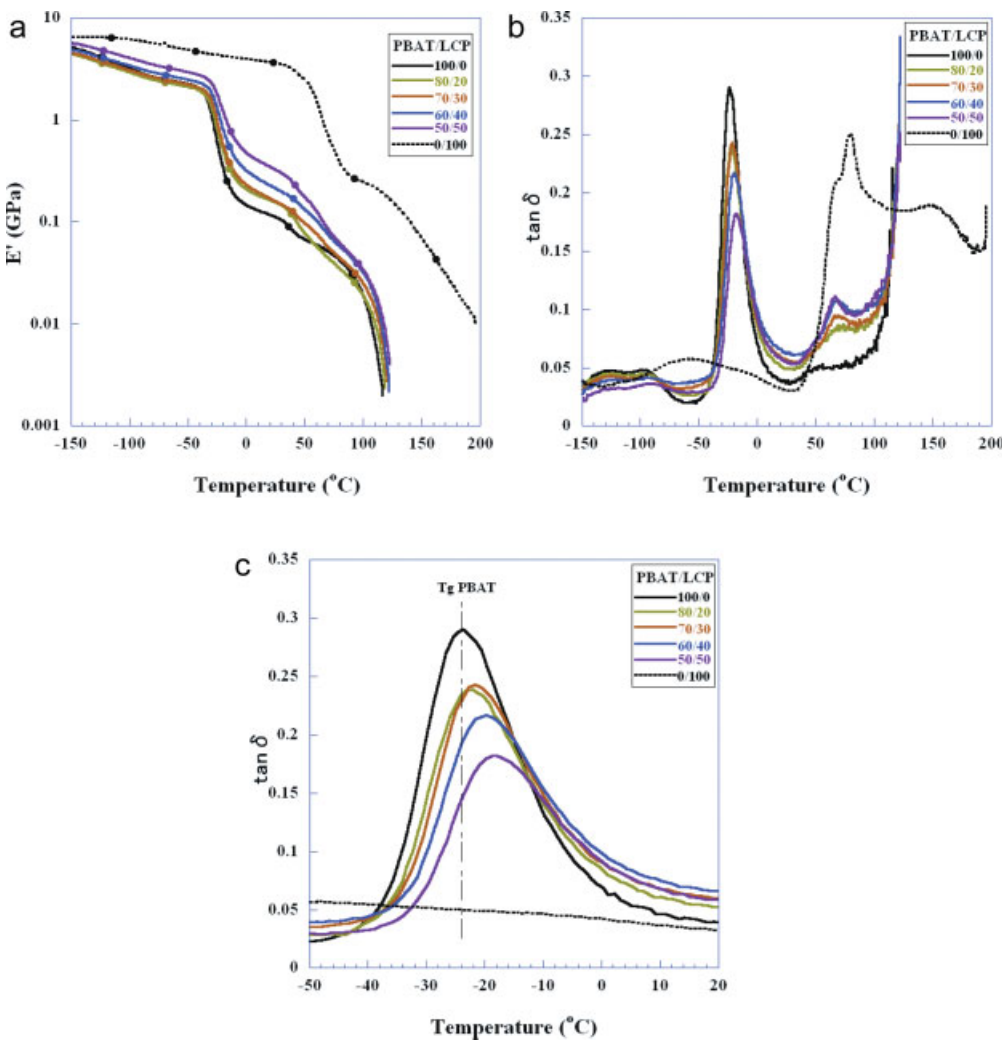

Figure 3 DMA results for pure PBAT, pure LCP, and PBAT/LCP blends (a) storage modulus, (b) tan δ, and (c) enlarged part of (b). [Color figure can be viewed in the online issue, which is available at www.interscience.wiley.com.]

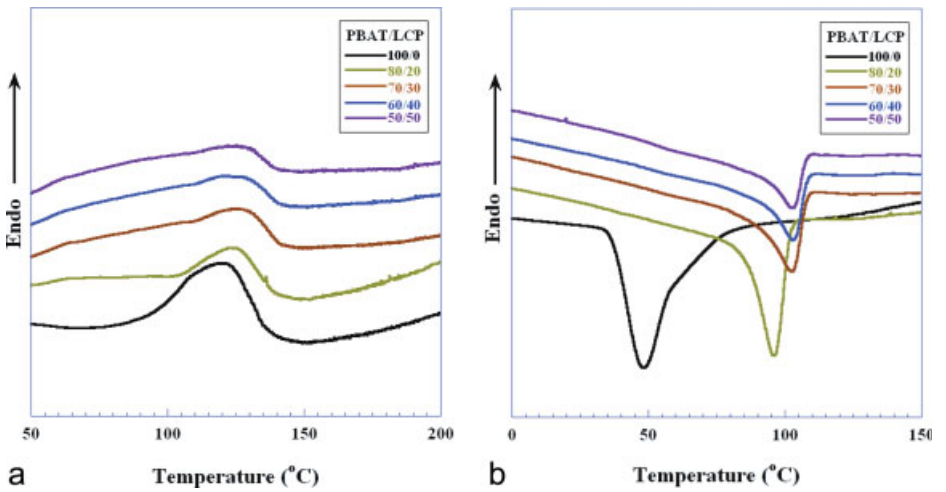

Figure 4 DSC curves of PBAT and PBAT/LCP blend: (a) melting endotherms, and (b) crystallization exotherms. [Color figure can be viewed in the online issue, which is available at www.interscience.wiley.com.]

domains. All the blends show typical sea-island morphologies, in which LCP domains are precisely dispersed in the PBAT matrix with a domain size of several micrometers. As the LCP composition increased, the LCP particle size of PBAT/LCP blends increases accordingly. It was found that the LCP domain size increased from 1 μm to about 3 μm when LCP composition increased from 20 to 50 wt %.

Thermal properties

The dynamic properties of the blended samples were characterized by DMA. The storage modulus E′ and loss tan δ for the blends with various compositions as a function of the temperature are shown in Figure 3. The storage modulus is directly related to the elastic response of the tested materials and tan δ is intimately associated with the chain relaxation that takes place. The storage modulus of the blends increases gradually in the entire temperature region with increasing LCP loading amount, indicating the clear strengthening effects of LCP on the PBAT matrix. Note that the glassy transition of PBAT occurs at about −23°C and that of LCP is located at about 79°C. It can be found that the T_g of PBAT is shifted from −23 to −17°C by increasing the LCP content. At the same time, the T_g of the LCP decreases from 79 to 66°C upon blending with PBAT. The shifted T_gs means that some molecular chain penetration occurs at the interface,[20–22] which indicates that PBAT shows good compatibility with LCP. This compatibility may have originated from the similar molecular structures of the ethylene terephthalate of LCP and the butylene terephthalate of PBAT.

The results of the DSC heating and cooling curves of the pure PBAT and the blends are shown in Figure 4(a,b), respectively, and the corresponding parameters, namely, melt temperature (T_m), crystallization temperature (T_c), and enthalpy of crystallization (ΔH_c), are presented in Table I. In the heating scan, the PBAT blends have slightly higher melting points than the neat PBAT. Figure 4(b) shows the DSC cooling curves for PBAT and PBAT/LCP blends. Apparently, the crystallization temperature

TABLE I
Thermal Properties of PBAT/LCP Blends

	T_m (°C)	T_c (°C)	ΔH_c (J/g)
PBAT	120.0	48.3	20.4
PBAT/LCP (=80/20)	124.7	96.0	14.9
PBAT/LCP (=70/30)	125.2	102.5	8.2
PBAT/LCP (=60/40)	124.7	103.0	7.9
PBAT/LCP (=50/50)	125.0	103.0	5.9

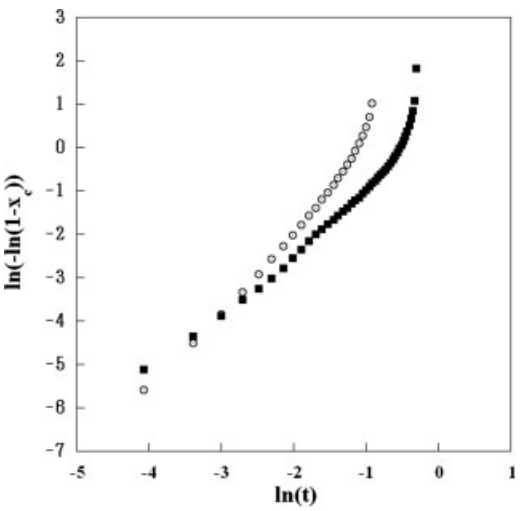

Figure 5 Avrami plots of PBAT crystallized from pure PBAT (○) and PBAT/LCP (=80/20) blend (■).

TABLE II
Crystallization Parameters for Pure PBAT and PBAT/LCP Blends

	n	logK
PBAT	2.48	2.96
PBAT/LCP (=80/20)	1.50	0.47
PBAT/LCP (=70/30)	1.54	0.34
PBAT/LCP (=60/40)	1.43	0.36
PBAT/LCP (=50/50)	1.34	0.17

(T_c) tends to shift to the high temperature region with increasing LCP content in the blends. The difference in crystallization peak temperature between pure PBAT and PBAT/LCP blends is as large as 45°C. It is considered that the LCP takes the nucleation agent role for PBAT during cooling down from the melt state. LCP shows good compatibility with the PBAT matrix. With decreasing temperature from the melt state of the blend, LCP solidifies first and PBAT starts crystallization from the surface of LCP. The same situation has also been reported for the PET/LCP and PBT/LCP systems. Sanjay et al. and Incarnato et al.[23,24] have shown the depression of PET crystallization temperature upon cooling in the presence of the LCP component. In addition, Sang and Bong[25] showed that the T_m of PBT decreases and its crystallization temperature increases with increasing amounts of LCP. They also found that the LCP acts as a nucleating agent for the crystallization of PBT. In addition, it can be found that the enthalpy of crystallization of PBAT decreases with increasing LCP contents, suggesting the good compatibility between the two components.

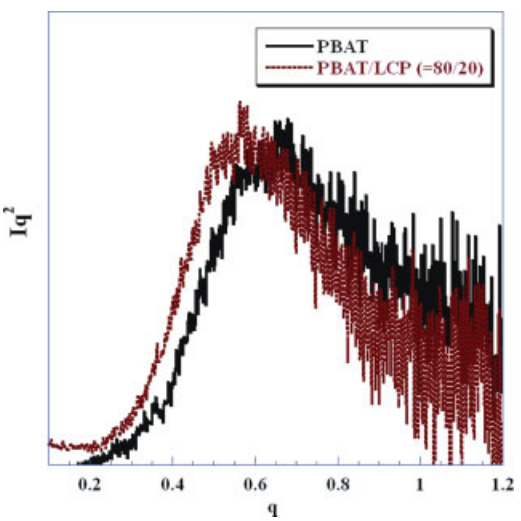

Figure 6 Lorentz-corrected SAXS profiles for pure PBAT and PBAT/LCP (=80/20) blend. [Color figure can be viewed in the online issue, which is available at www.interscience.wiley.com.]

The significant effects of LCP on the crystallization behavior of PBAT were further investigated on the basis of the isothermal crystallization kinetics. The experiments on the crystallization kinetics of pure PBAT and PBAT/LCP blends were carried out using the same procedure. The well-known Avrami equa-

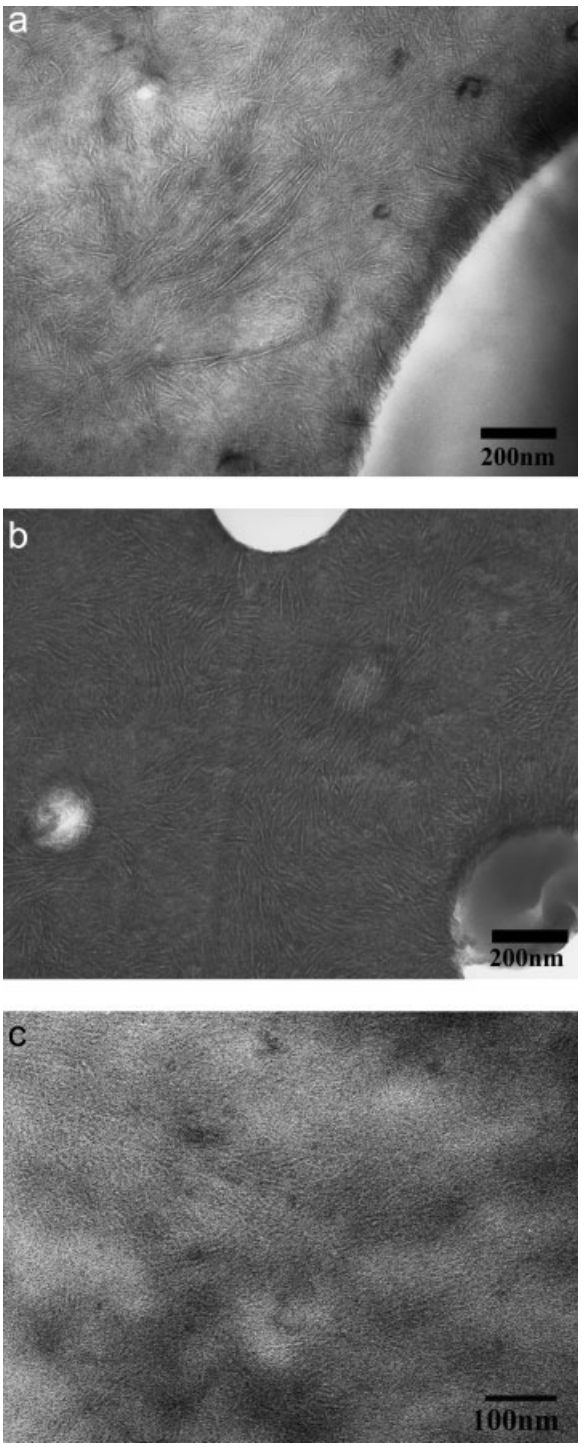

Figure 7 TEM micrographs for the PBAT/LCP blends: (a) PBAT/LCP (=50/50), (b) PBAT/LCP (=80/20), and (c) pure PBAT.

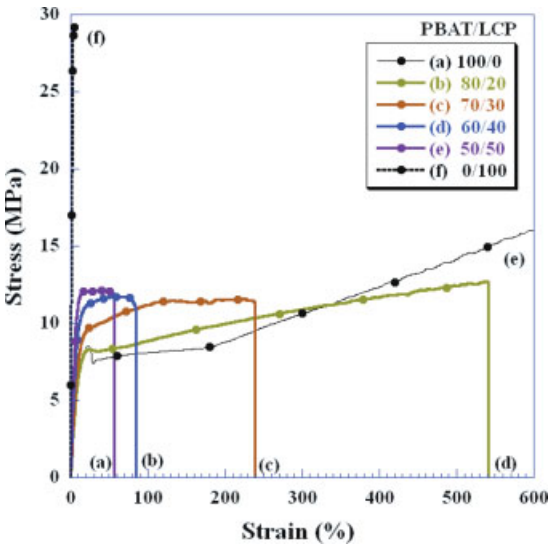

Figure 8 Stress–strain curves for PBAT/LCP blends: (a) PBAT/LCP (=50/50), (b) PBAT/LCP (=60/40), (c) PBAT/LCP (=70/30), (b) PBAT/LCP (=80/20), (e) pure PBAT, and (f) LCP. [Color figure can be viewed in the online issue, which is available at www.interscience.wiley.com.]

tion[26] was used to determine the characteristic parameters of polymer nucleation and crystal growth, as follows:

$$\mathrm{Log}\{-\ln(1 - X_t)\} = n \log t + \log K,$$

where t is the crystallization time, X_t is the relative degree of crystallinity at t, and n is the Avrami exponent, which depends on the nucleation and growth geometry of the crystals, K is the crystallization rate constant. The plots of log $\{-\ln(1 - X_t)\}$ against log$t$ for the pure PBAT and the typical PBAT/LCP blends with the composition ratio of 80/20 are shown in Figure 5. The decrease in n from 2.48 for the pure PBAT to 1.50 for the PBAT/LCP (=80/20) blend indicates that the nucleation mechanisms the two samples are different. For the blends, PBAT crystals nucleate from the interface and growth vertical to the interface, which gives a lower Avrami component. In contrast, pure PBAT can only nucleate from the impurity inside and gives a three-dimensional crystal growth. The crystallization parameters from Avrami analysis of the blend with various compositions are tabulated in Table II. It is shown that the Avrami exponents of the all blends are almost same, but smaller than that of the pure PBAT, indicating the clear nucleation effects of the LCP domains for the PBAT matrix.

Crystal morphology

We have shown that the addition of LCP has significant effects on the crystallization kinetics of PBAT. It is therefore interesting to investigate the lamellar structure of the PBAT crystals. Figure 6 shows the Lorentz-corrected SAXS profiles of pure PBAT and the PBAT/LCP (=80/20) blend. The SAXS intensity was normalized by thickness and exposure time after subtracting air scattering from the observed profiles. The pure PBAT exhibits a scattering peak at q = 0.67 nm^{-1}, corresponding to long periods of L = 9.3 nm. On the other hand, the PBAT/LCP (=80/20) blend shows a scattering peak at q = 0.56 nm^{-1}, corresponding to long periods of L = 11.1 nm. The crystal long period for PBAT crystals in the blend is longer than in the pure PBAT, which may be attributed to the higher crystallization temperature in the blend due to the nucleation effects of LCP domains.

The direct observation of the crystal lamellar structure of PBAT has been performed using high magnification TEM micrographs, as shown in Figure 7. The PBAT crystal lamellae can be clearly observed in the blends. Moreover, most of the lamellae are perpendicular to the interface between the PBAT matrix and LCP domains. It is considered that LCP domains can act as nucleates during the crystallization of PBAT, which is also suggested by the DSC results. In contrast, the lamellar structure of pure PBAT is very fine and is hardly to be seen, as shown in Figure 7(c). The difference in the crystal lamellar long period for the blend and pure PBAT from the TEM images is consistent with the results from SAXS measurements. The PBAT lamellae are observed to become thicker with increasing LCP content.

TABLE III
Tensile Properties of PBAT/LCP Blends

	Tensile modulus (MPa)	Yield strength (Mpa)	Tensile strength (Mpa)	Maximum strength (Mpa)	Strain at break (%)
PBAT	71	8.55	–	25.1	>600
PBAT/LCP (=80/20)	91	–	12.7		542
PBAT/LCP (=70/30)	104	–	11.6	–	240
PBAT/LCP (=60/40)	154	–	11.7	–	85.0
PBAT/LCP (=50/50)	195	–	12.2	–	56.5
LCP	1280	–	29.3	–	5.0

Mechanical properties

It is very interesting to study the mechanical properties of the PBAT/LCP blends. The tensile test results in the form of the stress–strain curves are shown in Figure 8. The tensile properties are also listed in Table III. The addition of LCP to PBAT increases the tensile strength and tensile modulus. Moreover, in PBAT/LCP blends, no tensile yield points can be observed. However, the elongation at the break decreases.

Figure 9 shows the stress–strain recovery behaviors of the pure PBAT and PBAT/LCP (=80/20) blend. The blend shows slightly better elastic recovery than the pure PBAT in spite of the addition of 20 wt % LCP to the PBAT phase.

To observe the effects of structure development during the injection molding of LCP-containing PBAT blends, SEM analysis was conducted. Figure 10 shows the morphology of the fracture surface of the composite. The sample was fractured perpendicular to the melt flow direction. This demonstrates that the LCP phase is elongated and finely dispersed in the PBAT matrix. The fibers are aligned along the melt flow direction. The diameter of the fibers is less than 1.5 μm.

CONCLUSIONS

We have successfully strengthened PBAT by simply melt blending with LCP. All blend samples exhibited marked improvements in mechanical properties such as tensile modulus and tensile strength. Moreover, the necking behavior upon stretching for neat PBAT diminished when blending with LCP. DSC results show that the crystallization rate of PBAT was increased significantly by addition of LCP and that the LCP dispersed domains act as nuclei for PBAT matrix. The nucleation effects of LCP on PBAT are attributed to the good compatibility between the two polymers.

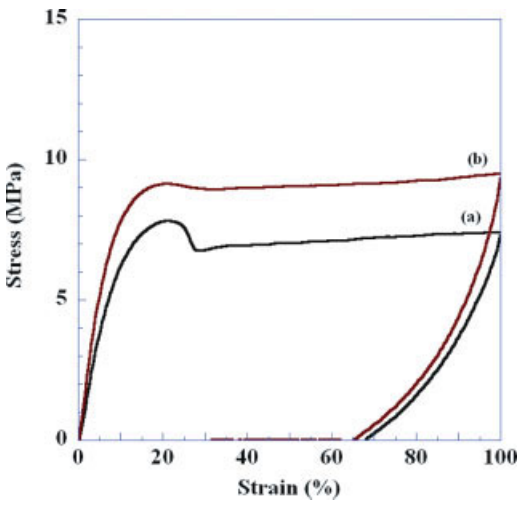

Figure 9 Strain recovery curves for (a) pure PBAT and (b) PBAT/LCP (=80/20) blend. [Color figure can be viewed in the online issue, which is available at www.interscience.wiley.com.]

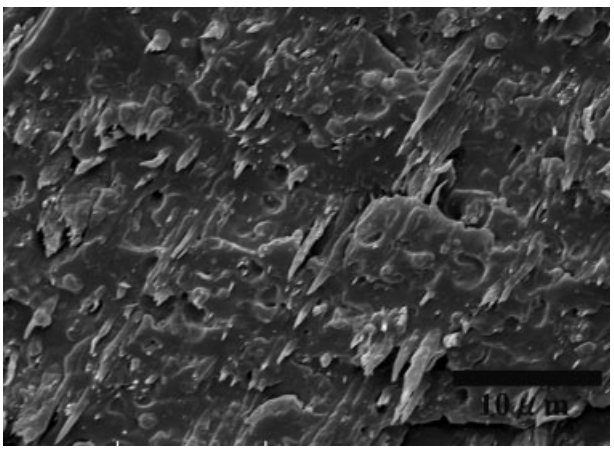

Figure 10 SEM micrograph of the PBAT/LCP (=60/40) blends after injection molded.

References

1. Doi, Y. Microbial Polyesters; VCH Publishers: New York, 1990.
2. Ikada, Y.; Tsuji, H. Macromol Rapid Commun 2000, 21, 117.
3. Sudesh, K.; Abe, H.; Doi, Y. Prog Polym Sci 2000, 25, 1503.
4. Yamashita, K.; Aoyagi, Y.; Abe, H.; Doi, Y. Biomacromolecules 2001, 2, 25.
5. Kikkawa, Y.; Abe, H.; Iwata, T.; Inoue, Y.; Doi, Y. Biomacromolecules 2001, 2, 940.
6. Muller, R.-J.; Kleenberg, I.; Deckwer, W.-D. J Biotechnol 2001, 86, 87.
7. Witt, U.; Einig, T.; Yamamoto, M.; Kleeberg, I.; Deckwer, W. D.; Müller, R. J. Chemosphere 2001, 44, 289.
8. Rantze, E.; Kleeberg, I.; Witt, U.; Müller, R. J.; Deckwer, W. D. Maromol Symp 1998, 130, 319.
9. Witt, U.; Müller, R. J.; Deckwer, W. D. Macromol Chem Phys 1996, 197, 1525.
10. Uwe, W.; Rolf-Joachim, M.; Wolf-Dieter, D. J Environ Polym Degrad 1995, 3, 215.
11. Witt, U.; Müller, R. J.; Deckwer, W. D. J Environ Polym Degrad 1997, 5, 81.
12. Shi, X. Q.; Ito, H.; Kikutani, T. Polymer 2005, 46, 11442.
13. Jiang, L.; Wolcott, M. P.; Zhang, J. Biomacromolecules 2006, 7, 199.
14. Yogaraj, U.; Nabar, D. D.; Ramani, N. J Appl Polym Sci 2006, 102, 58.
15. Rahman, M. H.; Nandi, A. K. Macromol Chem Phys 2002, 203, 653.
16. Bernstein, R. E.; Paul, D. R.; Barlow, J. W. Polym Eng Sci 1978, 18, 1225.
17. Becke, R. E.; Cabasso, I. Polymer 1988, 29, 1831.
18. Jun, Y.; Kim.; Seong, H. K. J Polym Sci Part B: Polym Phys 2005, 43, 3600.
19. Jun, Y.; Kim.; Seong, H. K. Polym Int 2006, 55, 449.
20. Chen, J. H.; Zhong, J. C.; Cai, Y. H.; Su, W. B.; Yang, Y. B. Polymer 2007, 48, 2946.
21. Vilics, T.; Schneider, H. A.; Manoviciu, V.; Manoviciu, I. J Thermal Analysis 1996, 47, 1141.
22. Qi, K.; Nakayama, K. J Mater Sci 2001, 36, 3207.
23. Sanjay, M.; Deopura, B. L. Polym Eng Sci 1993, 33, 931.
24. Incarnato, L.; Motta, O.; Acierno, D. Polymer 1998, 39, 5085.
25. Sang, H.; Bong, S. K. Polym Eng Sci 1995, 35, 528.
26. Avarami, M.; J Chem Phys 1939, 24, 1103.